SUPPLEMENTARY INFORMATION

Nanoengineering 2D Ceria-Perovskite Monolayers on $SrTiO_3$ Nanocubes: Structure-Redox Property Relationship

*Ramón Manzorro, Jose M. Montes-Monroy, Carmen Mora-Moreno, Lidia E. Chinchilla, Ana B. Hungría, Jose J. Calvino, and Jose A. Pérez-Omil**

Departamento de Ciencia de los Materiales e Ingeniería Metalúrgica y Química Inorgánica, Facultad de Ciencias, Universidad de Cádiz, 11510-Puerto Real, Spain
Instituto de Microscopía Electrónica y Materiales (IMEYMAT), Facultad de Ciencias, Universidad de Cádiz, 11510-Puerto Real, Spain

* Email: jose.perez-omil@uca.es

X-Ray Diffraction

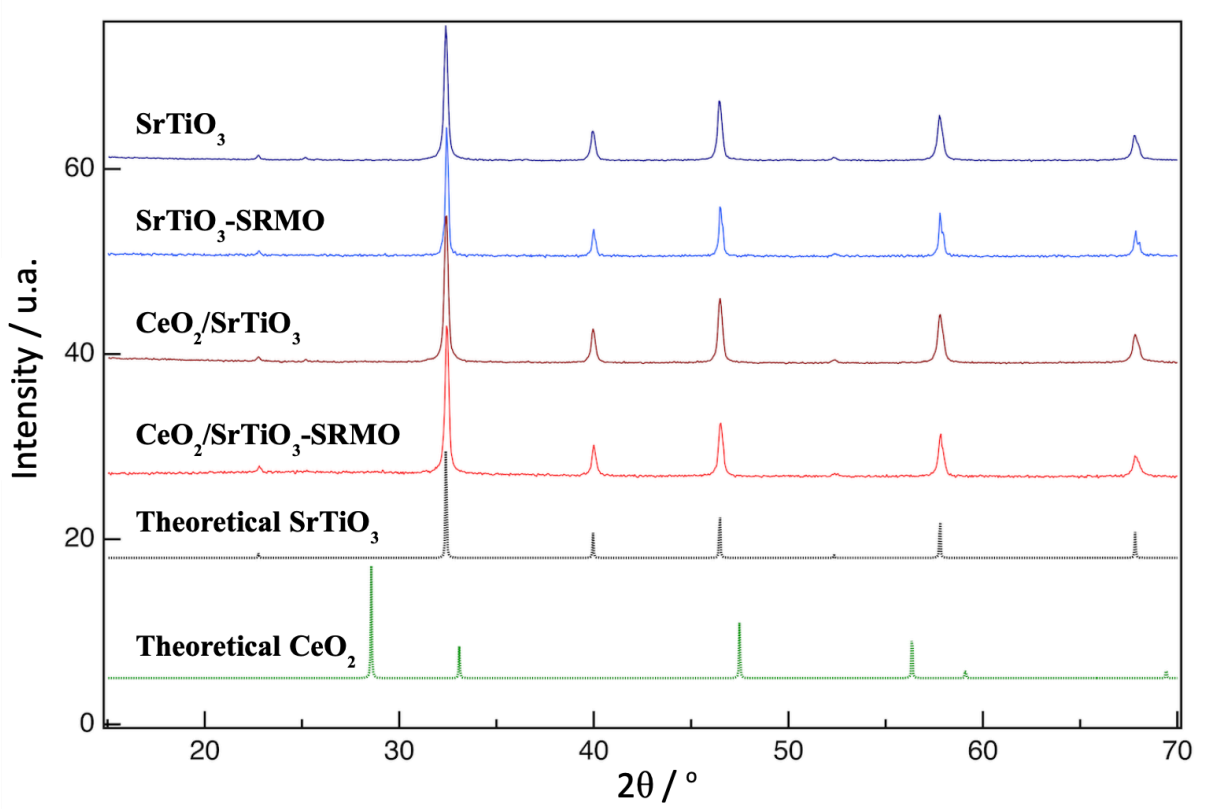

Figure S1. *X-ray diffractograms are shown corresponding to the $SrTiO_3$, $SrTiO_3$-SRMO, $CeO_2/SrTiO_3$ and $CeO_2/SrTiO_3$-SRMO samples (from top to bottom, respectively). Theoretical X-ray diagrams of the $SrTiO_3$ (black) and CeO_2 (green) phases are also included.*

In-depth $SrTiO_3$ morphology

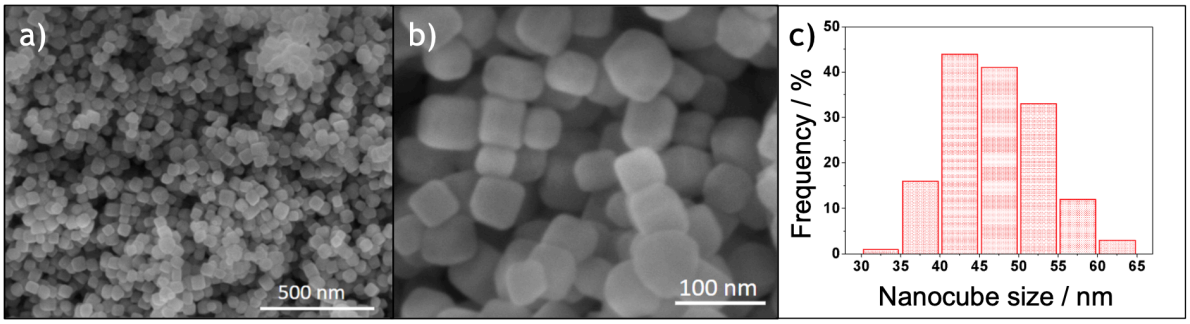

***Figure S2**. Morphology of $SrTiO_3$ support. a) and b) SEM images at different magnifications showing the shape and size of the nanocubes. c) Particle size distribution measured from over 100 nanocubes.*

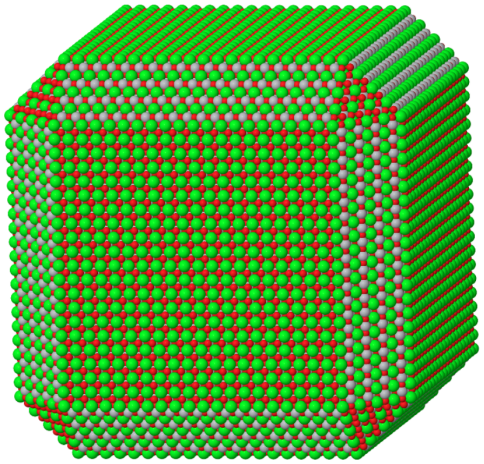

***Figure S3**. An atomic model of a nanocube, built in Rhodius, is shown based on the {001}, {110} and {111} planes. These planes correspond to the faces, the edge bevels and the corners of the cube, respectively.*

X-Ray Photoemission Spectroscopy

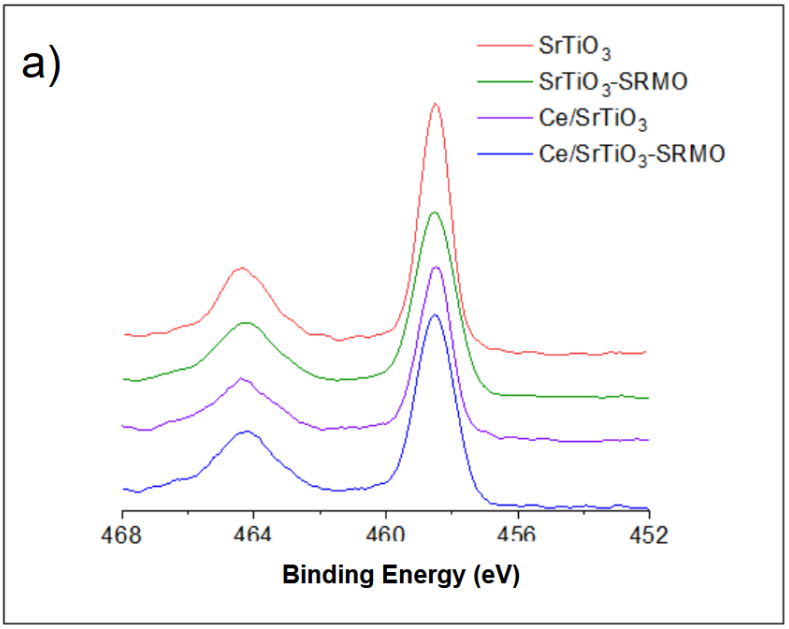

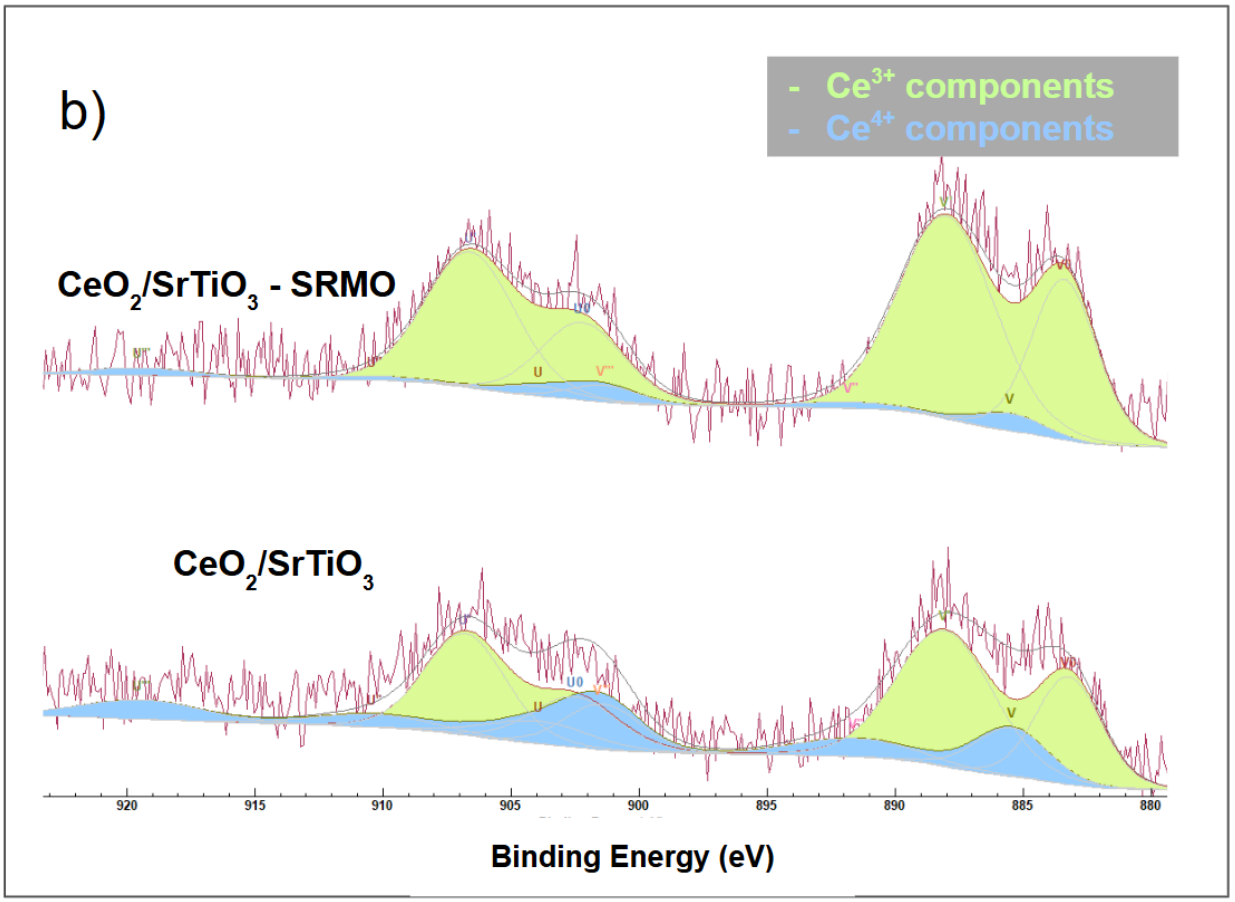

***Figure S4**. (a) XPS spectra of Ti 2p signal for $SrTiO_3$, $SrTiO_3$-SRMO, $CeO_2/SrTiO_3$ and $CeO_2/SrTiO_3$-SRMO samples (from top to bottom). The two peaks appear at the same binding energies, that is 458.5 and 464.2 eV for the Ti 2p 3/2 and Ti 2p 1/2 excitations, which are characteristic of Ti^{4+}. This finding indicates that reduced titanium is not detected after the ceria deposition or following the SRMO treatment. (b) XPS spectra of Ce 3d signal for $CeO_2/SrTiO_3$-SRMO and $CeO_2/SrTiO_3$ samples (from top to bottom). These XPS signals indicate that the Ce is greatly reduced in all samples. This is very likely due to the highly-reducible nature of the low-loading, nanostructured, surface ceria combined with the sample manipulation and exposure to X-rays during the experiments. However, the presence of Ce^{4+} suggests that the sample was initially oxidized. Qualitatively, the spectra also indicate that the SRMO-treated sample exhibits higher reducibility than the fresh counterpart.*

Mass spectrometry during redox experiments

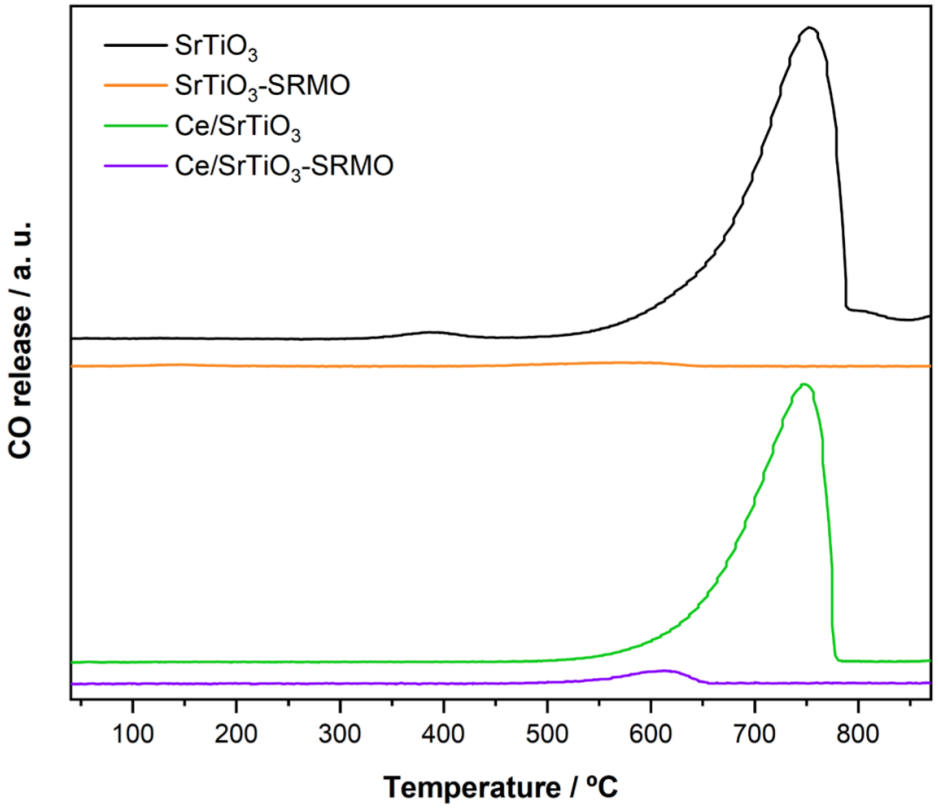

***Figure S5**. The CO signal (m/z=28) registered on the mass spectrometer is shown. The profiles correspond, from top to bottom, to $SrTiO_3$, $SrTiO_3$-SRMO, $CeO_2/SrTiO_3$ and $CeO_2/SrTiO_3$-SRMO samples.*

$SrTiO_3$ atomic resolution crystal structure

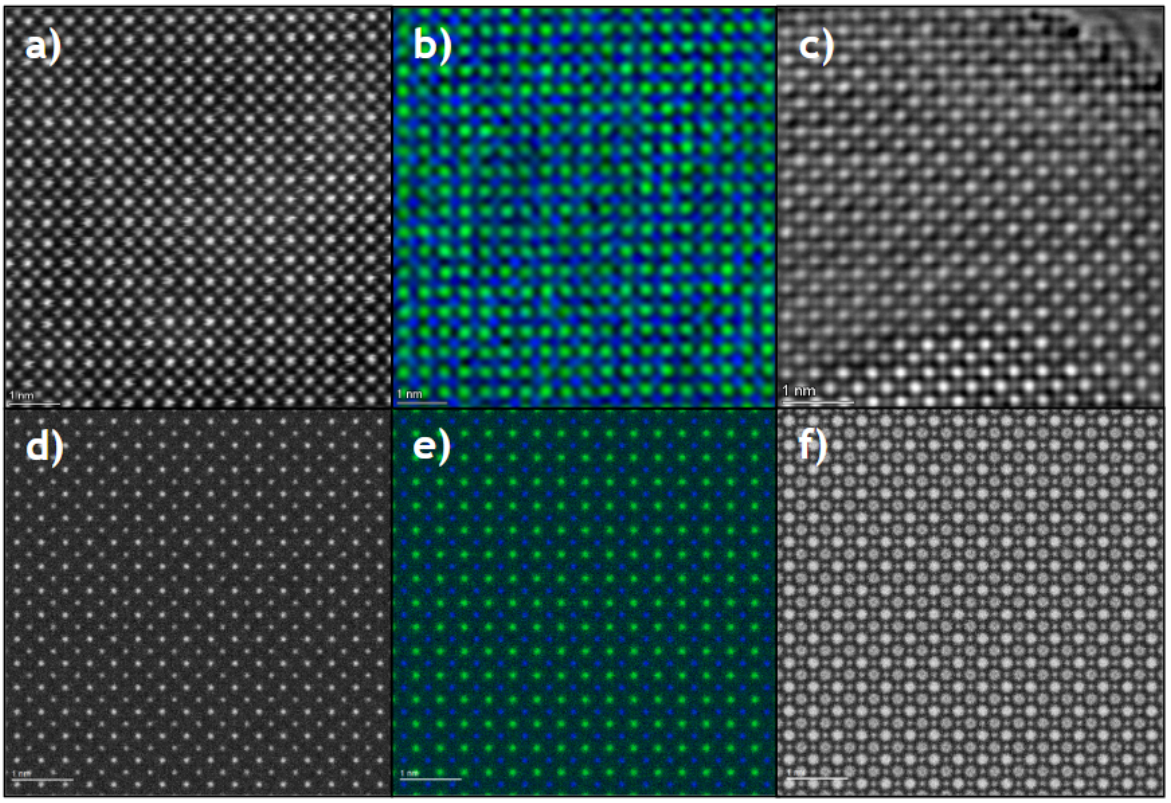

***Figure S6**. Atomic resolution characterization of $SrTiO_3$ nanocubes confirming the perovskite structure. a) HAADF image, b) XEDS elemental map, with Ti and Sr shown in green and blue colours respectively, confirming the typical cationic arrangement of this structure along the [001] zone axis. c) iDPC image where the oxygen columns are visualized. d) ,e) and f) represent the simulated HAADF, XEDS and iDPC images, respectively. These simulations were performed using the μSTEM program considering a model with a thickness of 200 Å and the following experimental conditions: 200 kV, 0.001 mm Cs3, 5 mm Cs5, 1nm defocus, 19 mrad convergence angle, 80-200 mrad HAADF angles and, 8-19 mrad segmented ADF angles for the iDPC image.*

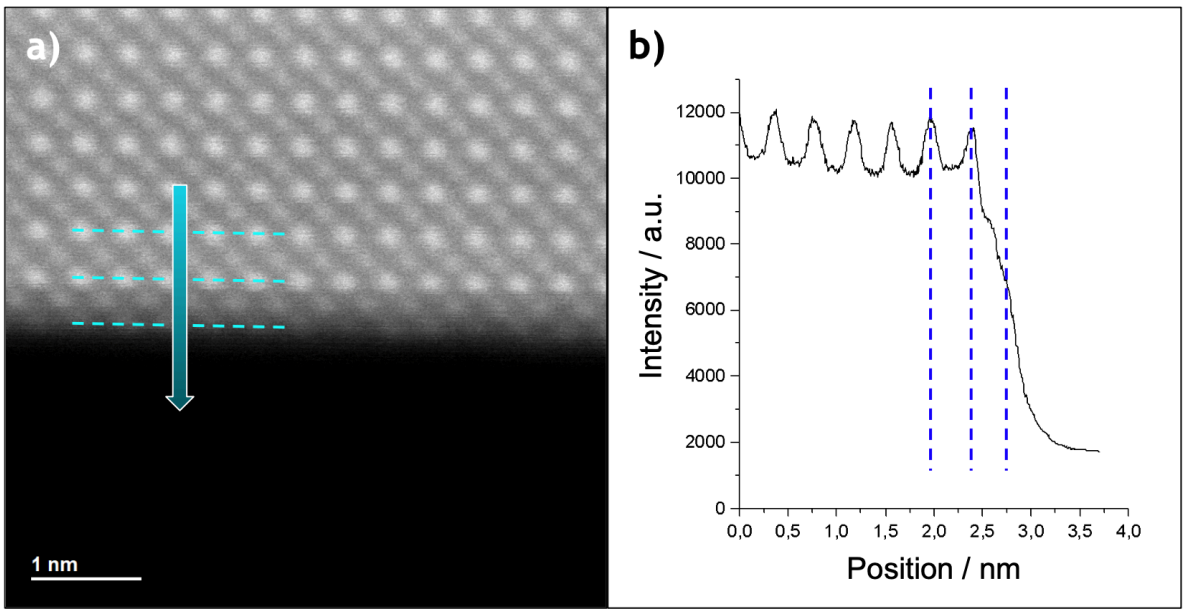

***Figure S7**. Surface analysis of $SrTiO_3$ nanocubes. a) HAADF image where a $SrTiO_3$ (001) surface is atomically resolved. b) Intensity profile plot following the blue arrow displayed in a).*

Structural relationships and DFT calculations

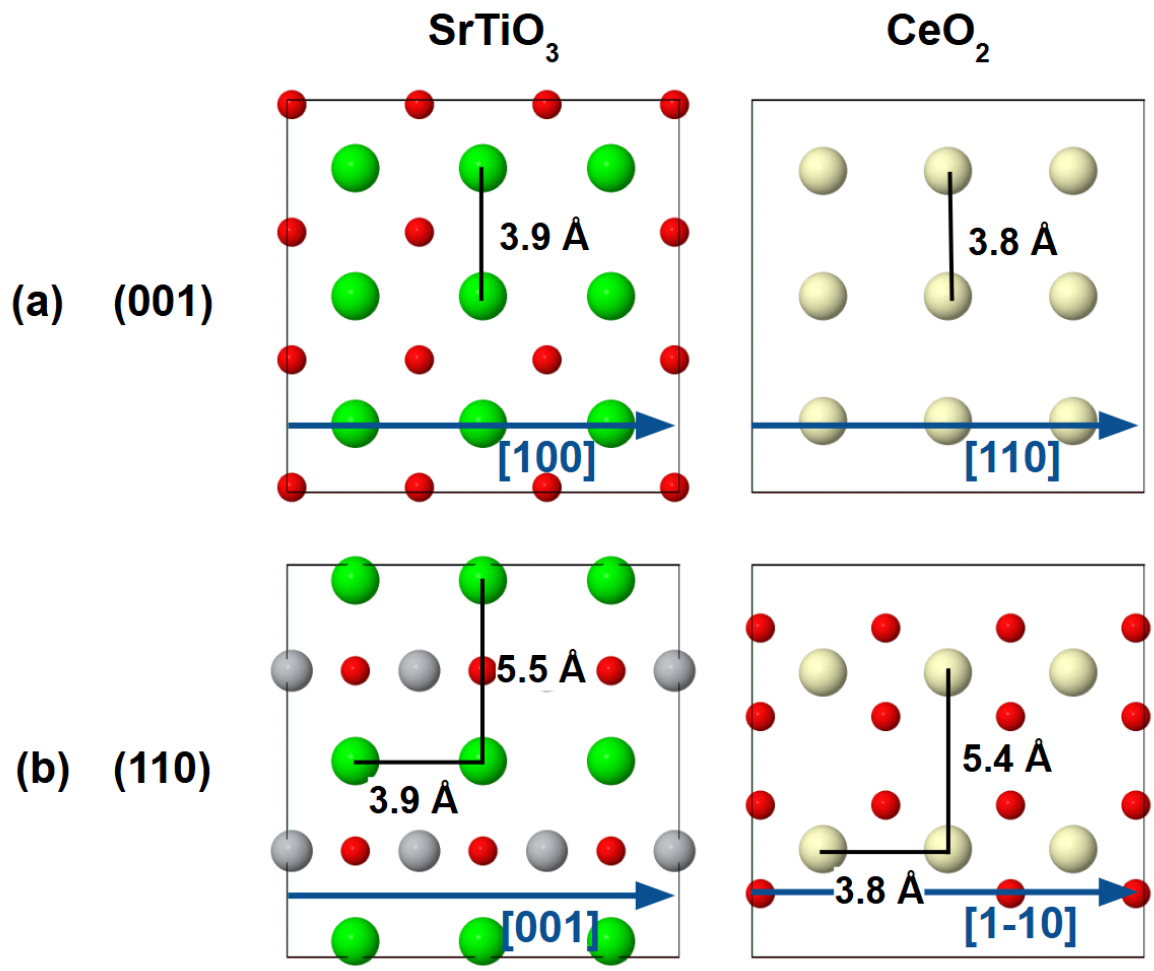

Figure S8*. Atomic surfaces of $SrTiO_3$ and CeO_2 representing the contact planes of each structural relationship. a) (001) planes for AA45 epitaxy. The CeO_2 [110] zone axis is aligned with the $SrTiO_3$ [100] zone axis, resulting in a 45º rotation between both structures. b) (110) planes for the BB90 epitaxy. The CeO_2 [1-10] zone axis is aligned with the $SrTiO_3$ [001] zone axis, resulting in a 90º rotation between both structures.*

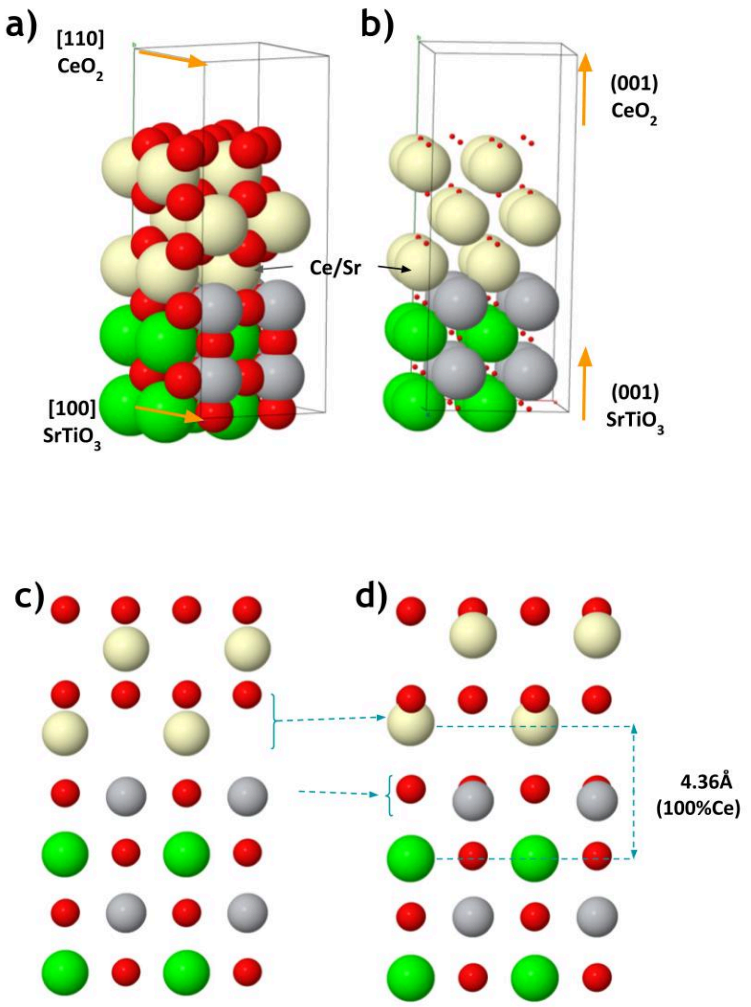

Figure S9. *Atomic models detailing the AA45 epitaxial relationship described as (001) CeO_2 // (001) $SrTiO_3$ and [110] CeO_2 // [100] $SrTiO_3$. Note that the initial cationic plane of the fluorite structure is a mixed layer of Ce and Sr. a) Atomic model visualizing the continuity of the cationic and anionic sublattices. b) The same atomic model focusing on the cation network to illustrate the continuity that occurs between the bcc Sr/Ti sub-lattice of the perovskite and the fcc Ce sub-lattice on the fluorite. Note that, in general, the bcc structure can be regarded as a tetragonally distorted fcc, or vice versa. c) and d) Atomic models of the (001) CeO_2/$SrTiO_3$ interface before and after the DFT relaxation, respectively. Notably, the interface relaxation leads to a tiny splitting of the last layer (TiO_2) in the perovskite structure. Simultaneously, the Ce and O_2 planes in the initial fluorite planes tend to merge into a single CeO_2 plane. There is an expansion from the last pure Sr plane and the mixed Ce/Sr layer that reaches the value of 4.36 Å when the occupancy of Ce atoms reaches 100%. Cerium, strontium, titanium, and oxygen atoms are represented by the colors beige, green, gray, and red, respectively.*

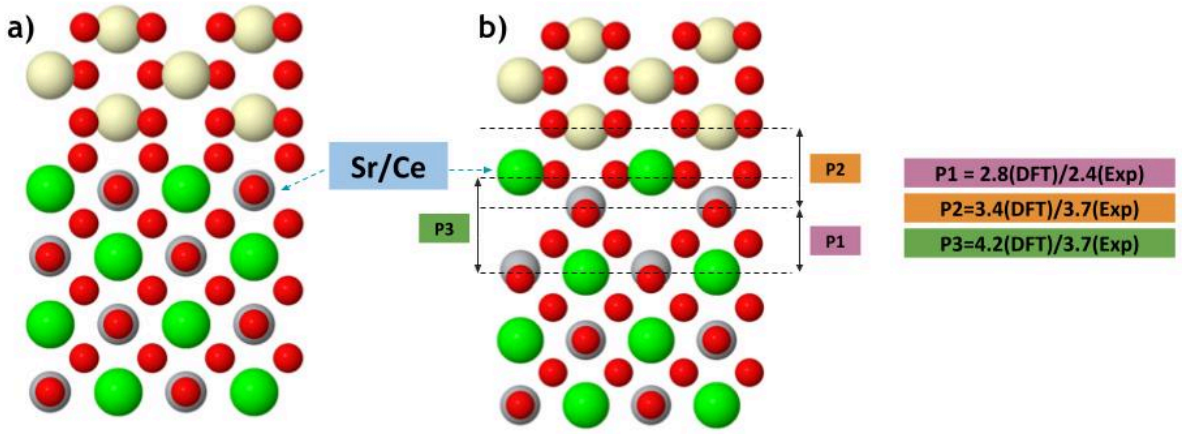

Figure S10. *Atomic models of the $CeO_2/SrTiO_3$ interface at the (110) planes of both structures are shown a) before and b) after the DFT relaxation. Similar to the AA45, the BB90 epitaxy also leads to a splitting that, in this case, occurs in the last SrTiO plane. This splitting results in the merging between Sr and O_2 planes giving rise to a SrO_2 plane that is isoestructural to fluorite. Simultaneously a TiO plane is generated immediately below the SrO_2 plane. The interface spacings (theoretically and experimentally) considered are: between the penultimate SrTiO plane of the perovskite structure and the new TiO plane (P1), between the first CeO_2 plane of the fluorite structure and the new TiO plane (P2) and between the penultimate SrTiO plane and the new SrO_2 plane (P3). These spacings have been indicated in b). For the sake of simplicity, it has been assumed that the Sr occupation in the last plane of the original SrTiO perovskite is 100%.*

EELS surface analysis

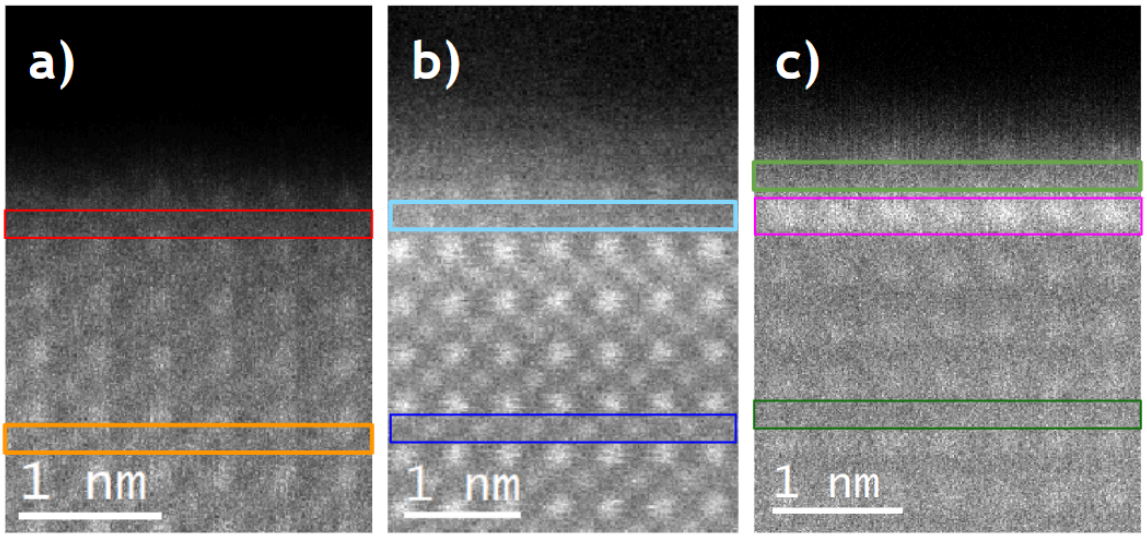

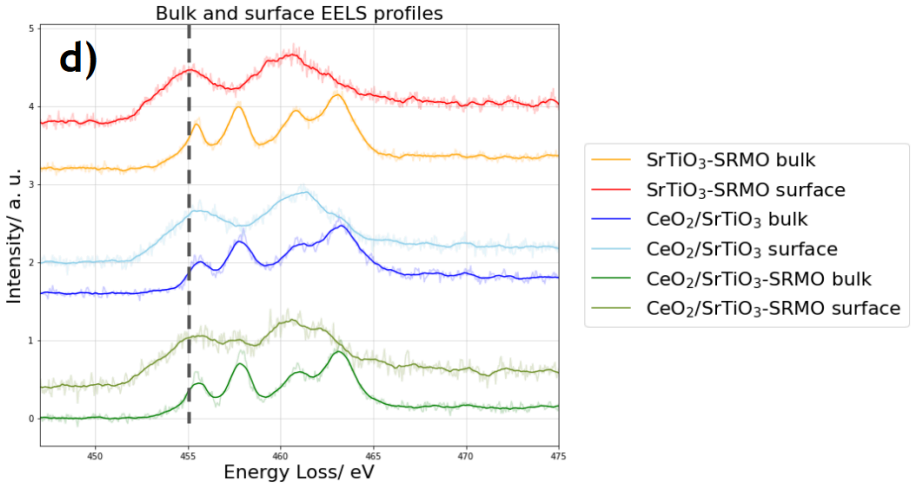

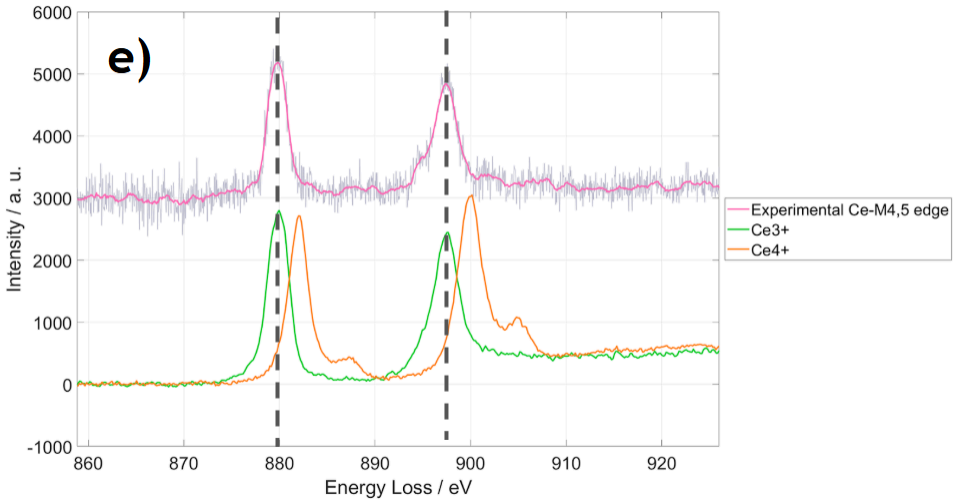

Figure S11. *Atomic-resolution Ti-$L_{2,3}$ EELS surface analysis. a), b) and c) represent the corresponding ADF images of the surfaces of $SrTiO_3$-SRMO, $CeO_2/SrTiO_3$ and $CeO_2/SrTiO_3$-SRMO samples, respectively. d) EELS fine structure comparing the bulk and surface Ti-$L_{4,5}$ edges for the cited samples. Bulk profiles are consistent with the presence of Ti^{4+}, while those at the surface exhibit a clear loss of the fine structure details and a red shift specifically for the $SrTiO_3$-SRMO sample. This features could be attributed to a combination of factors: the decrease of symmetry and coordination number of the atoms right on the surface, some amorphization and reduction of the sample by the effect of the electron beam or the presence of inherent Ti^{3+} at the surface. e) EELS fine structure comparing the surface Ce-$M_{4,5}$ edge for the $CeO_2/SrTiO_3$-SRMO sample and the reference spectra for Ce^{4+} and Ce^{3+}. The Energy Loss Near-Edge Structure (ELNES) reveals that cerium is present predominantly as Ce^{3+}. This is attributed to electron beam-induced reduction, facilitated by the highly dispersed nature of the ceria phase, although the presence of residual Ce^{4+} cannot be entirely excluded; these findings are in good agreement with the XPS results. Note: The color of each spectrum corresponds to its respective acquisition area as indicated by the colored boxes in the HAADF images, with the exception of the reference spectra.*

Atomic models for DFT calculations to explore the formation of the Ce-monolayer

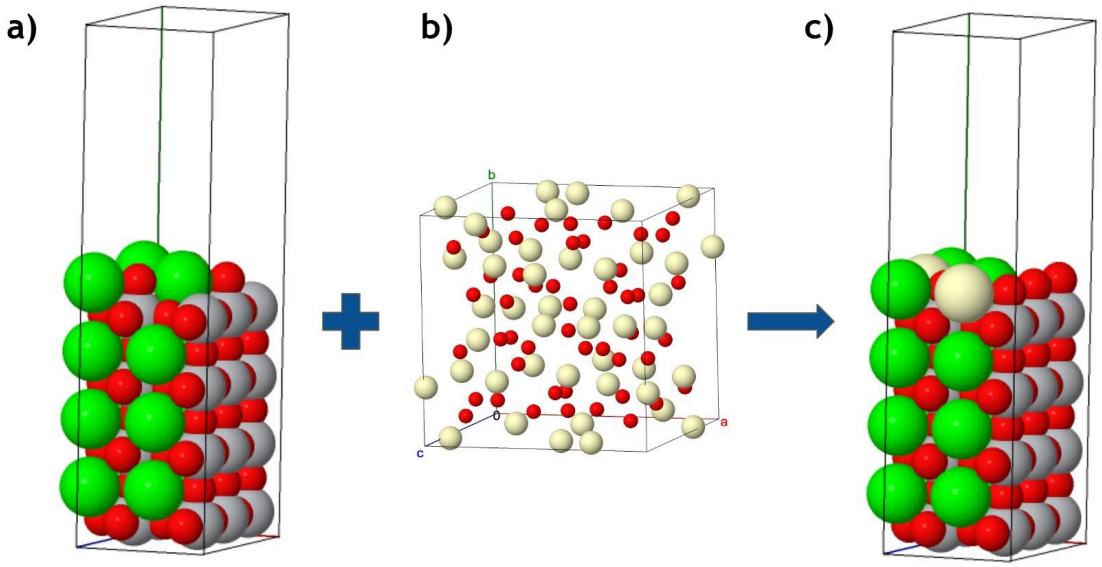

***Figure S12**. Atomic models proposed to elucidate the formation of the Ce/Sr monolayer during the reduction treatment. a) Atomic model of pure $SrTiO_3$ where the (001) surface is terminated with a half-layer of SrO. b) Cubic unit cell for the C-Ce_2O_3 structure. c) Atomic model containning three layers of $SrTiO_3$ at the bottom and one layer of $Sr_{1/2}Ce_{1/3}TiO_3$ (the so called Ce/Sr-layer) at the surface. Note that for every six original Sr positions, three are occupied by Sr (occupancy: ½) and two are occupied by Ce (occupancy: ⅓), leaving one cationic vacancy (occupancy: ⅙). It is not necessary to include oxygen vacancies in the final model. The absolute energies calculated after relaxation of the supercells are U_{SrTiO3} , E_{Ce2O3} and $U_{SrCeTiO3}$, respectively. A +3 oxidation state for Ce was assumed in all DFT calculations.*

IL-STEM and *in situ* studies of the Ce-rich layer formation

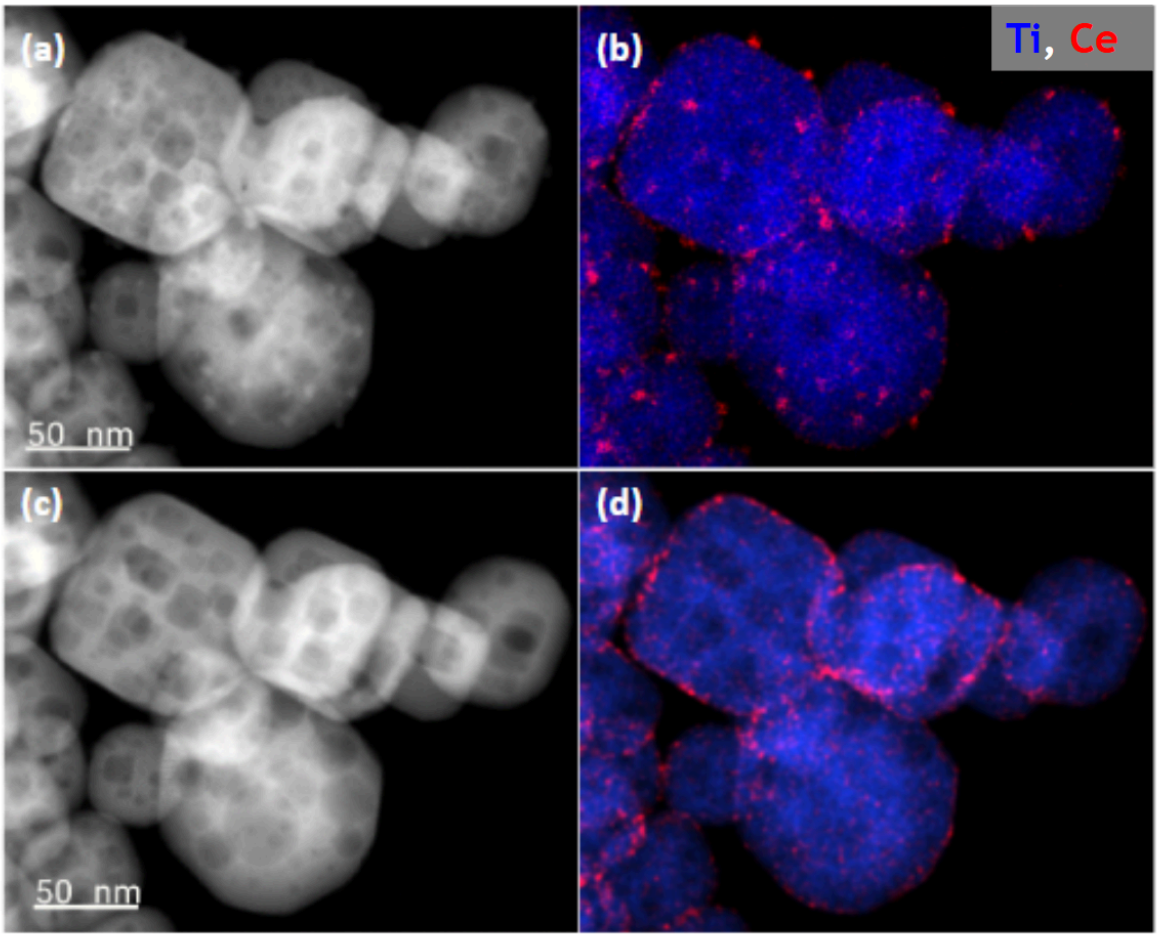

Figure S13. *IL-STEM characterization at medium magnification. a) and b) show the HAADF image and XEDS elemental map of the CeO_2/$SrTiO_3$ sample, whic clearly indicates the presence of nanometer-sized CeO_2 nanoparticles. c) and d) HAADF image and XEDS map of the same area after the SRMO treatment (CeO_2/$SrTiO_3$-SRMO sample), revealing how nanoparticles have spread across the $SrTiO_3$ surface. The elements titanium and cerium are represented in blue and red colours, respectively, in the XEDS maps.*

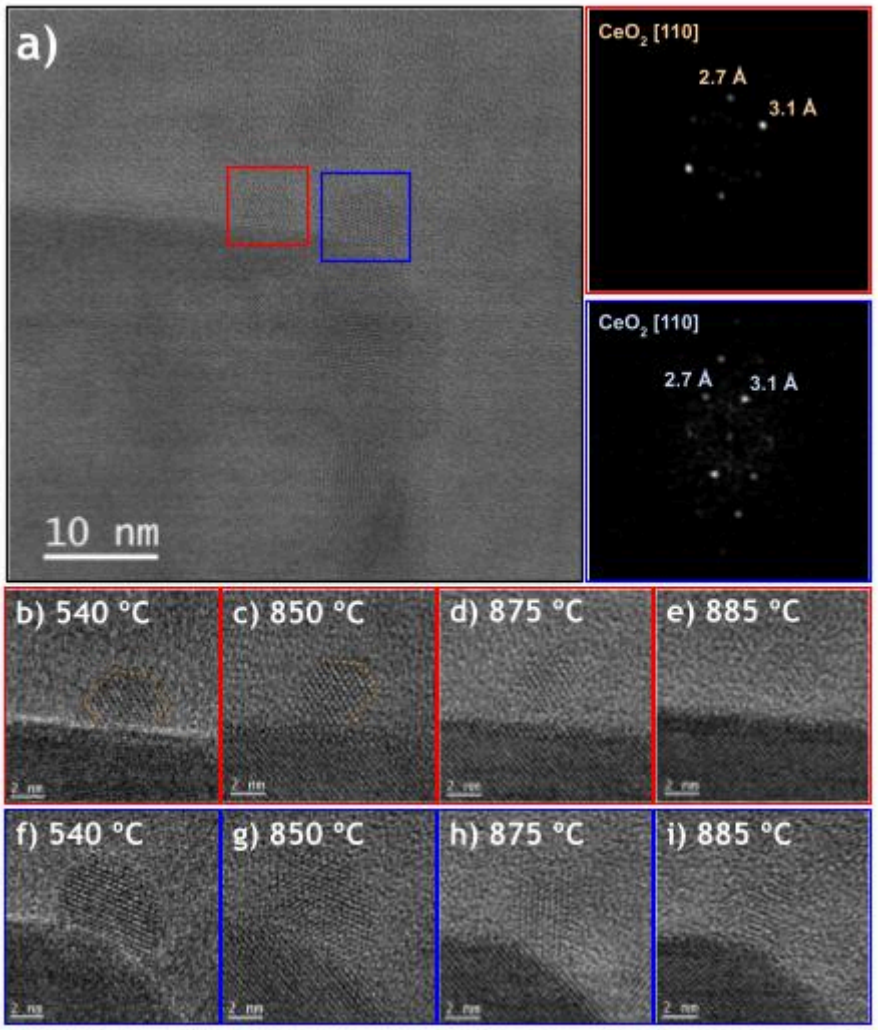

***Figure S14**. In situ characterization of a CeO_2 nanoparticle during the SR stage of the SRMO treatment. a) HRTEM image of a $SrTiO_3$ nanocube with a couple of supported CeO_2 nanoparticles. The FFTs of both nanoparticles (red and blue squares) confirm the fluorite structure oriented along the [110] crystallographic direction. b)-e) and f)-i) show a sequence of TEM images of the CeO_2 nanoparticles while the temperature is increased from 500 to 900 °C. Specifically, the image-series capture the temperatures 540, 850, 875 and 885 °C, unveiling the progressive disappearance of the CeO_2 nanoparticles when the temperature exceeds 850 °C.*

Atomic models for DFT+U calculations to explore the formation of just one Ce-monolayer

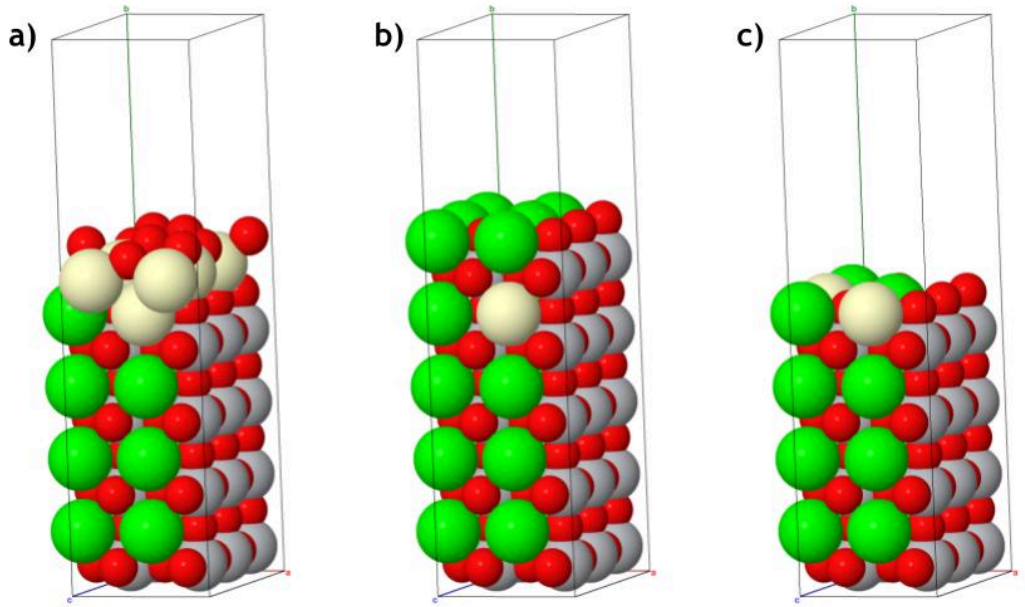

***Figure S15**. Atomic models considered to understand the formation of just one monolayer of the lanthanide phase. a) Atomic model containning three layers of $SrTiO_3$ at the bottom, one layer of $Sr_{1/2}Ce_{1/3}TiO_3$ (the so called Ce/Sr-layer) and one layer of C-Ce_2O_3 on top. b) The same model as before, but the reduced ceria is substituted by a $SrTiO_3$ layer (the so called Sr-Ti double layer). c) Atomic model where the surface just ends in the Ce/Sr-layer, without any other layer on top. The absolute energies calculated after relaxation of the supercells are $U_{Ce2O3/SrCeTiO3}$, $U_{SrTiO3/SrCeTiO3}$ and $U_{SrCeTiO3}$, respectively. The oxidation state of the element Ce considered in the calculations is +3.*